Automatic Detection of Airstrips in the Amazon Using ICEYE SAR Imagery and U-Net Neural Networks

Gustavo Henrique de Queiroz Stabile[1], Dimas Irion Alves[1], Tahisa Neitzel Kuck[2], Paulo Ricardo Branco da Silva [1] e Saleh Javadi [3]

[1] Instituto Tecnológico de Aeronáutica (ITA), São José dos Campos/SP – Brazil

[2]Instituto de Estudos Avançados (IEAv), São José dos Campos/SP – Brazil

[3]Blekinge Institute of Technology, Karlskrona - Sweden

***Abstract*— This study investigates convolutional neural networks, specifically the U-Net architecture, for the automated detection of irregular airstrips in the Amazon rainforest using Synthetic Aperture Radar (SAR) imagery from ICEYE satellites operating in the X-band. Detecting these airstrips is strategic for combating illicit activities and protecting the environment. SAR imagery is particularly effective in the Amazon, as it can penetrate cloud coverage, which is common in the region. A comprehensive pipeline was developed for data preparation, model training, and evaluation, utilizing the airstrips cataloged by the MapBiomas project for reference. Experiments were conducted by varying both the size of the input images and the balance of the training dataset. Results indicated that even with a limited number of images, the U-Net architecture can generate consistent outcomes. The study supports the development of operational solutions for the automated monitoring of irregular airstrips in the Amazon region.**

***Keywords*— Synthetic Aperture Radar, automatic detection, Deep Learning, airstrips.**

I. Introduction

The detection of airstrips in the Amazon region is a task of growing significance for government agencies and institutions focused on environmental protection [1], [2]. These structures, often constructed secretly, are used for the illegal transportation of goods and the unauthorized exploitation of natural resources [3], [4]. Systematic monitoring of these airstrips can help combat illicit activities and protect sensitive areas.

The vast expanse of the Amazon region and its challenging accessibility make field-based monitoring difficult and expensive. In this context, spaceborne remote sensing is vital in collecting information to support government actions [5]. However, the Amazon region also presents challenges for these systems. Its climate, characterized by high humidity and temperatures, favors cloud formation, which obstructs the acquisition of optical images for much of the year [6].

To address this issue, the Brazilian Air Force acquired ICEYE satellites through the Lessonia Project to capture Synthetic Aperture Radar (SAR) images of the Earth's surface [7]. SAR technology allows for image acquisition regardless of cloud cover or lighting conditions, which is especially beneficial in the Amazon region [8].

Once the SAR images are acquired, the next major challenge lies in processing this vast volume of data to identify airstrips effectively. The complexity arises from the need to distinguish small, often narrow linear structures in heterogeneous landscapes, such as forests, rivers, and rural clearings. In recent years, numerous studies have demonstrated the potential of SAR imagery in the automatic detection of diverse targets, including vehicles, ships, and buildings, by applying advanced image processing and Artificial Intelligence (AI) techniques [9], [10], [11]. These methods leverage the inherent advantages of SAR, such as its robustness to adverse weather and lighting conditions, enabling consistent surveillance in environments like the Amazon, where cloud cover and limited ground access hinder traditional monitoring. Convolutional Neural Networks (CNNs), in particular, have shown high effectiveness in learning spatial and textural patterns from SAR data, making them suitable for segmentation and classification tasks involving man-made infrastructure embedded in complex natural scenes [12].

Research on the detection of airstrips remains relatively scarce in the existing literature. Recent studies have employed Sentinel-1 SAR data for this purpose, leveraging its free availability and extensive coverage [13]. However, these studies often encounter challenges due to the sensor's spatial resolution, which is approximately 10 meters. This resolution particularly complicates the identification of narrow and elongated structures, such as irregular airstrips, especially in densely vegetated or partially degraded regions. In many cases, airstrips can be narrower than 20 meters, further complicating their detection at this resolution [14]. For instance, [15] proposed an improved algorithm for detecting airstrips in the Amazon rainforest using multi-stage filtering and object analysis in optical images, while [13] applied a YOLOv8-based deep learning approach to Sentinel-1 imagery for the same task. While these studies make significant contributions, they remain preliminary. Additionally, those utilizing SAR images depend on medium spatial resolution data, which restricts the accuracy and reliability of the detections. This gap presents a significant opportunity to advance the state of the art through the utilization of high-resolution SAR imagery, such as that provided by ICEYE satellites. By leveraging finer spatial details and the capabilities of convolutional neural

G.H.Q. Stabile, stabile@ita.br; D.I. Alves, dimasirion@ita.br; T.N. Kuck, tatakuck@gmail.com; P.R.B. Silva, pauloricardo.branco@gmail.com; S. Javadi, saleh.javadi@bth.se. This work was supported by FINEP (grant number 01.22.0581.00), the National Institute of Science and Technology (INCT-Signals), which is funded by Brazil's National Council for Scientific and Technological Development (CNPq) under grant number 406517/2022-3, the Ministry of Science, Technology, and Innovation (MCTI), and the São Paulo Research Foundation (FAPESP) under grant 20/09838-0 (BI0S—Brazilian Institute of Data Science).

networks, we can enhance both the sensitivity and precision of airstrip detection in complex and remote environments like the Amazon.

This paper aims to fill gaps identified in previous research by examining the characteristics of images that exhibit poor detection performance, primarily focusing on the Intersection over Union (IoU) metric. Additionally, we will describe our efforts to enhance the masking process used for generating ground truth data. Finally, we will analyze key hyperparameters that seem to be intrinsically connected to detection performance, including the balance of training data and image resolution.

This paper is structured as follows: Section II describes the methodology, the dataset, along with the preparation process for images and segmentation masks and the network architecture used; Section III presents the results and corresponding analyses; finally, Section IV discusses the conclusions and directions for future work.

II. Methodology

This section outlines the methodological approach developed for detecting airstrips in the Amazon using X-band SAR imagery from satellites combined with Deep Learning techniques. It begins with a description of the pre-processing stage, primarily focusing on the construction of the dataset. This includes the selection and annotation of images, as well as the generation of segmentation masks. Additionally, the section provides an overview of the U-Net convolutional neural network architecture along with details on its implementation. Finally, the experimental setup is discussed, covering the image processing stage, training strategies, evaluation metrics, and the criteria used to assess the model's performance.

A. Dataset

The dataset used in this study consists of SAR images collected by ICEYE satellites and supplied by the Institute for Advanced Studies (IEAv). This research institution, affiliated with the Brazilian Air Force, plays a strategic role in the development of aerospace technologies and remote sensing capabilities. The ICEYE satellite operates in the X-band and generates VV-polarized SAR images in various acquisition modes, with spatial resolutions ranging from 0.25m to 15m [16]. For this work, images captured in Stripmap mode with a spatial resolution of 3 meters per pixel were chosen to create the dataset. The selected images were acquired during the years 2022 and 2023.

To complement the SAR imagery selected for this study, reference data on known airstrip locations were required to support supervised learning and ground truth generation. For this purpose, georeferenced information on airstrips in the Amazon region was obtained from the MapBiomas project published in 2023 [17].

This study analyzed optical imagery of the Amazon region from the year 2021 to identify and catalog airstrips and compare them with official Brazilian government records. A total of 2,869 airstrips were identified in the area, with 1,205 (42%) registered with the National Civil Aviation Agency and 1,664 (58%) unregistered. Each airstrip was cataloged with various attributes; for this study, the unique identifier (ID) and geographic coordinates of a reference point on each airstrip were utilized.

To ensure spatial alignment between the reference data and the radar imagery, a cross-referencing step was performed between the airstrip catalog and the SAR dataset. This step was essential to isolate only those instances where the annotated airstrips were fully covered within the available SAR scenes, enabling the extraction of consistent and valid samples for further analysis.

After cross-referencing the airstrip database with the available SAR images, we retained only those airstrips that appeared in at least one SAR image. As a result, only 244 airstrips remained, representing approximately 8.5% of the total cataloged airstrips. Fig. 1 displays a map of the Amazon region, with blue rectangles representing the SAR image areas and orange circles representing the cataloged airstrips used in this study.

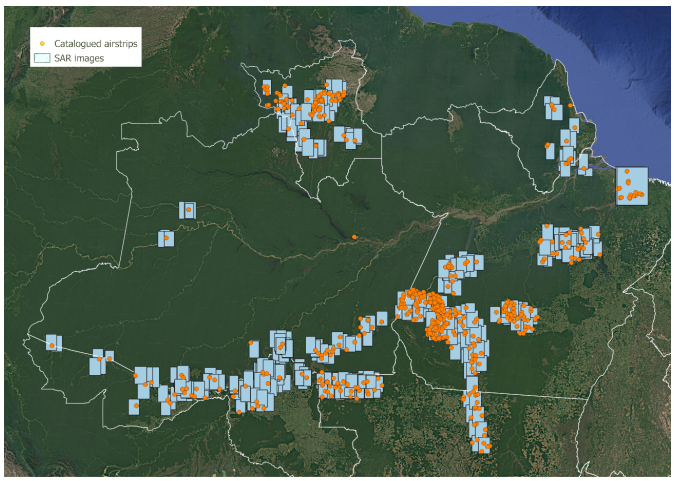

Fig. 1. Map of the Amazon region with SAR image contour and airstrips.

For each airstrip, a 2 × 2 km square area centered on the reference coordinate was extracted from the original SAR image, isolating the airstrip and its surroundings as a sample for neural network training. The 2km dimension was selected based on the typical length of airstrips observed in the region, which are generally shorter than 2 km, ensuring that the entire structure is captured within the subset image.

To train the segmentation model, each SAR image subset required a corresponding annotation indicating the airstrip location. To ensure spatial alignment between the SAR data and the optical references, a coregistration procedure was performed to verify the alignment of the masks relative to the SAR image geometry. Binary masks were then created with polygons covering the entire surface of each airstrip. Fig. 2 displays an optical image with a red square indicating the subset image boundaries and a green rectangle outlining the airstrip.

To ensure the quality and relevance of the training data, additional criteria were applied during sample selection. Only image patches that fully contained at least one annotated airstrip were retained. This selection aimed to preserve the distinctive characteristics of airstrips, which exhibit clearly defined start and end points, making it possible to differentiate them from other linear structures, such as roads and rivers.

As a result of this process, the final dataset included 640 images corresponding to 244 distinct airstrips. The number of

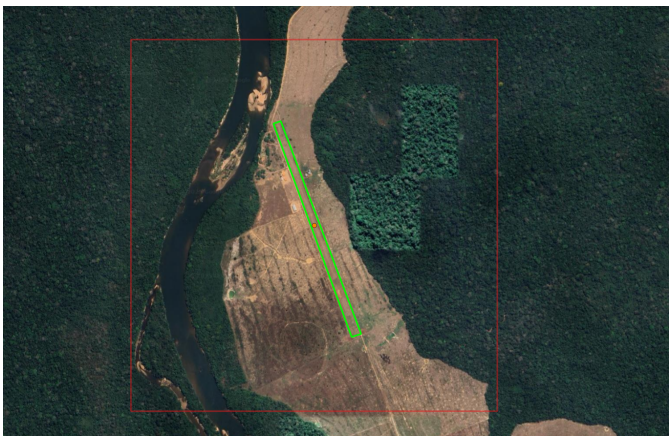

Fig. 2. Example of optical image with airstrip polygon.

samples per airstrip varied from 1 to 15, with 123 airstrips represented by only one sample and one airstrip represented by 15 samples. Fig. 3 shows the distribution of the number of available images per airstrip.

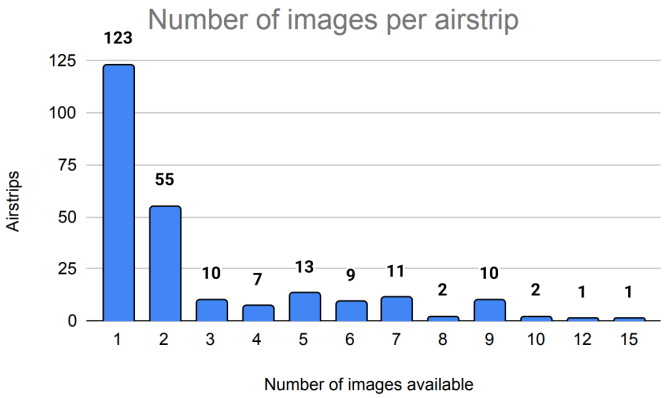

Fig. 3. Number of images per airstrip ID.

From the total set, 12 airstrips were selected to form a control group for qualitative monitoring of the network's performance. These airstrips were chosen based on visual criteria, focusing on airstrips that were distinguishable from the surrounding terrain. This approach was intended to ensure consistent and interpretable evaluations of the model's predictions. The remaining airstrips were divided into training, validation, and test groups, with a distribution of 70%, 20%, and 10%, respectively, as outlined in [18]. To prevent data leakage between groups, only airstrips represented by a single image were included in the validation, test, and control sets.

B. Neural Network Architecture: U-Net

The architecture employed is based on U-Net, a convolutional neural network widely used for image segmentation tasks [19]. It is recognized for its capacity to produce precise segmentations, even with a limited amount of labeled data.

The U-Net architecture features a U-shaped design, comprising two primary components: the encoder and the decoder. The encoder conducts hierarchical feature extraction through convolutional and pooling operations, gradually decreasing the spatial resolution of the representations. The decoder reconstructs the segmentation from the compressed representations by utilizing upsampling and convolutional layers to restore the original spatial resolution.

A key element of U-Net is the use of skip connections between corresponding layers of the encoder and decoder, which facilitate the transfer of detailed spatial information [19]. These connections are crucial for refining the edges and contours of the segmented regions, as they allow the decoder to recover spatial resolution and preserve fine structural details lost during downsampling. This improved reconstruction of the segmentation is particularly important for airstrip detection [20], [21].

In this study, a U-Net version proposed in [14] was implemented, adhering to the original structure presented in [19], with modifications such as batch normalization and ReLU activation following each convolutional layer.

The architecture consists of four encoder blocks, each containing two convolutional layers with 3×3 kernels and ReLU activation, followed by batch normalization. Each block is followed by 2×2 max pooling, which reduces spatial resolution by a factor of 2 in each dimension and, consequently, reduces the number of pixels per channel by 4, all the while doubling the number of filters, beginning with 64 filters and reaching 512. A transition block (bridge) with 1024 filters connects the encoder and decoder, representing the network's deepest level and its most abstract data representation.

The decoder consists of four blocks. Each block begins with an upsampling layer that utilizes transposed convolution, which doubles the spatial resolution while halving the number of filters. The upsampled feature map is concatenated with the corresponding encoder output through skip connections, allowing for the recovery of spatial information lost during pooling. This is followed by two convolutional layers, each accompanied by batch normalization and ReLU activation.

The output layer features a 1×1 convolution with softmax activation, generating a segmentation map with two classes per pixel: "target" and "background". The choice of softmax activation over sigmoid was made due to its slightly better performance in a comparable segmentation task, as noted in [14].

C. Experimental Setup

The configuration adopted for the experiments was based on parameters previously validated in related work [14], including the network architecture, batch size, optimizer, and loss function. A batch size of 8 images was used to balance memory efficiency and training stability, while the Adam optimizer was selected for its robustness and widespread adoption in image segmentation tasks. The Dice Loss function was chosen due to its effectiveness in handling class imbalance, a common challenge in semantic segmentation [22]. The number of training epochs was set to 200, based on preliminary experiments which indicated that the loss function on the validation set typically stabilized around epoch 100.

The evaluation metric used in this study is Intersection over Union (IoU). The IoU metric is particularly effective for assessing pixel-wise detection performance, as it directly measures the overlap between the predicted mask and the ground truth. Given the two-dimensional nature of the segmentation problem, achieving a perfect match across an

entire region can be inherently challenging, especially in scenarios with complex backgrounds and subtle features of the target. Therefore, pixel-level evaluation provides a more realistic and equitable assessment of the model's performance. The intersection with ground truth pixels serves as a critical indicator of detection quality, reflecting not only the presence of the target but also the spatial accuracy of the segmented regions.

The configurations for training and for performance validation are shown in Table I.

TABLE I

TRAINING CONFIGURATION DETAILS

Parameter	Value
Network architecture	U-Net
Batch size	8 images
Number of epochs	200
Optimizer	Adam
Loss function	Dice Loss
Metrics	Intersection over Union (IoU)

Results were evaluated based on the Dice loss function and the IoU metric on the test set, in addition to the number of detections. The Dice loss used for training and testing is defined as:

$$\mathcal{L}_{\text{soft-Dice}}(\mathbf{X}, \mathbf{Y}) := 1 - \frac{2 \sum_{i=1}^{N} \langle \hat{\mathbf{Y}}_i, \mathbf{Y}_i \rangle + \varepsilon}{\sum_{i=1}^{N} \|\hat{\mathbf{Y}}_i\|_1 + \sum_{i=1}^{N} \|\mathbf{Y}_i\|_1 + \varepsilon}, \quad (1)$$

where:

- $\mathbf{X}_i \in \{0, \ldots, 2^\delta - 1\}^{H \times W \times C}$ denote the i-th quantized input image,
- $\hat{\mathbf{Y}}_i = f_{\text{U-Net}}(\mathbf{X}_i; \boldsymbol{\theta}) \in [0, 1]^{H \times W}$ denote the predicted mask (before thresholding),
- $\mathbf{Y}_i \in \{0, 1\}^{H \times W}$ denote the corresponding binary ground-truth mask.
- $\langle \hat{\mathbf{Y}}_i, \mathbf{Y}_i \rangle = \sum_{h=1}^{H} \sum_{w=1}^{W} \hat{Y}_i(h, w) Y_i(h, w)$ is the Frobenius inner product (i.e., soft intersection),
- $\|\cdot\|_1$ denotes the element-wise 1-norm (sum of all tensor elements),
- $\varepsilon > 0$ is a small constant added for numerical stability to avoid division by zero.

A valid detection was defined as an overlap of at least 30% between the predicted area and the ground truth mask. The 30% overlap threshold was defined to favor the detection of potential airstrips, even in cases of partial segmentation, since in this application false positives are preferable to missed detections, which could result in overlooking strategically relevant targets in remote areas. Moreover, as demonstrated in [14], the correct segmentation of even small sections of an airstrip is often sufficient to enable its identification, given their characteristic linear geometry and contextual cues in the surrounding terrain. Fig. 4 illustrates an example of a successful detection, with Fig. 4 (a) displaying the original SAR image, 4 (b) the ground truth mask, and 4 (c) the network's predicted mask.

III. Results and Discussion

Initially, experiments were conducted varying the image resolution. The original images have a resolution of approximately 800 × 800 pixels; tests were performed using higher resolution (1024×1024) and lower resolutions (512 × 512 and 256 × 256). The images were converted to 8 bits, as shown by [15], to reduce computational costs and enhance the contrast between image elements.

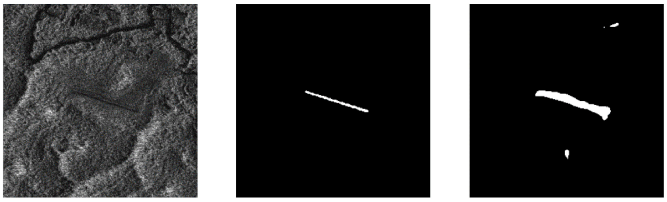

(a) Original image (b) Truth mask (c) Predicted mask

Fig. 4. Example of a successful detection.

The results indicated a small difference in performance between the 256 and 512 pixel resolutions; however, the 1024 resolution resulted in significantly worse performance. As shown in Table II, when using all available images, the 256 resolution yielded an average test loss of approximately 84% and an IoU of 8%, while the 512 resolution resulted in an 83% loss and a 6.5% IoU. The test with 1024 resolution presented a 92% loss and 0% IoU. This loss of performance at higher resolution may be attributed to the limited number of training samples available, which can lead to overfitting or insufficient generalization, as larger images introduce a higher number of parameters and spatial variability, demanding more data to train the model effectively.

TABLE II

COMPARISON OF RESULTS BY IMAGE RESOLUTION

Resolution (px)	Test Loss	Test IoU
256	0.8439245	0.0788340
512	0.8310944	0.0645017
1024	0.9189511	0.0000000

The imbalance in the number of samples per airstrip was a concern throughout this study. The limited data volume required a careful balance between maximizing the number of images used and maintaining network performance.

To assess the impact of dataset imbalance, tests were conducted using both the complete dataset and datasets with the number of samples per airstrip limited to between 1 and 6 images. The results showed that, when using very few images per airstrip, the network struggled to learn effectively, resulting in random predictions. Fig. 5 presents the test loss and IoU results for networks trained with different numbers of samples per airstrip. All tests were performed at a resolution of 256 × 256 pixels, selected based on previous experiments that indicated slightly better performance at this resolution compared to others, while also offering reduced computational cost.

Limiting the training set to 6 images per airstrip produced more accurate outcomes, with a loss of approximately 79% and a 9.8% IoU, indicating that the network effectively learned the characteristics of the target objects. Fig. 6 illustrates an example of performance improvement as the number of samples per airstrip changes. Fig. 6 (a) represents the ground truth mask, while Fig. 6 (b) to (g) show predictions from networks trained with sample limits from 1 to 6, respectively. Fig. 6 (h) displays the prediction from the network trained with the complete dataset. The test with the training group

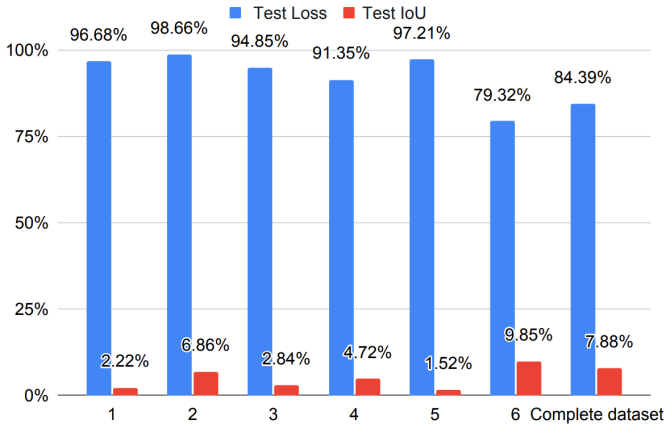

Fig. 5. Results with different limits on the number of samples per airstrip.

limited to 6 images per airstrip achieved better performance than using the full dataset, with only 51 images discarded, providing an appropriate balance between dataset balance and total data volume.

Repeating the resolution variation test for datasets with limited samples per airstrip, the results indicated that using lower-resolution images is feasible without significant loss of performance. This approach can be beneficial for reducing computational costs and training time. The importance of dataset balance became evident when, even with a small dataset, limiting the number of images per target improved the network's final performance. A possible explanation for this effect is that an excessive number of samples from a few specific airstrips may cause the network to overfit to their visual characteristics, reducing its ability to generalize to other targets. By capping the number of samples per airstrip, the training data becomes more evenly distributed across different examples, promoting better feature diversity and enhancing the network's generalization capability. Finding this balance point is crucial, especially when working with limited data.

An analysis of the prediction results reveals that the network had difficulty segmenting airstrips located in areas with low vegetation or deforested terrain. Figure 7 (a) shows the original SAR image, where there is a noticeable low contrast between the airstrip and its surroundings. In Figure 7 (c), which displays the mask predicted by the network, it is clear that the predicted feature corresponds to the forest edge near the airstrip rather than the actual target. This suggests confusion between vegetation boundaries and linear structures.

It is also important to note that the segmentation masks were based on optical satellite imagery. Although a visual coregistration process was applied, minor misalignments between the SAR and optical data may have contributed to inaccuracies in labeling, especially in low-contrast or heterogeneous regions.

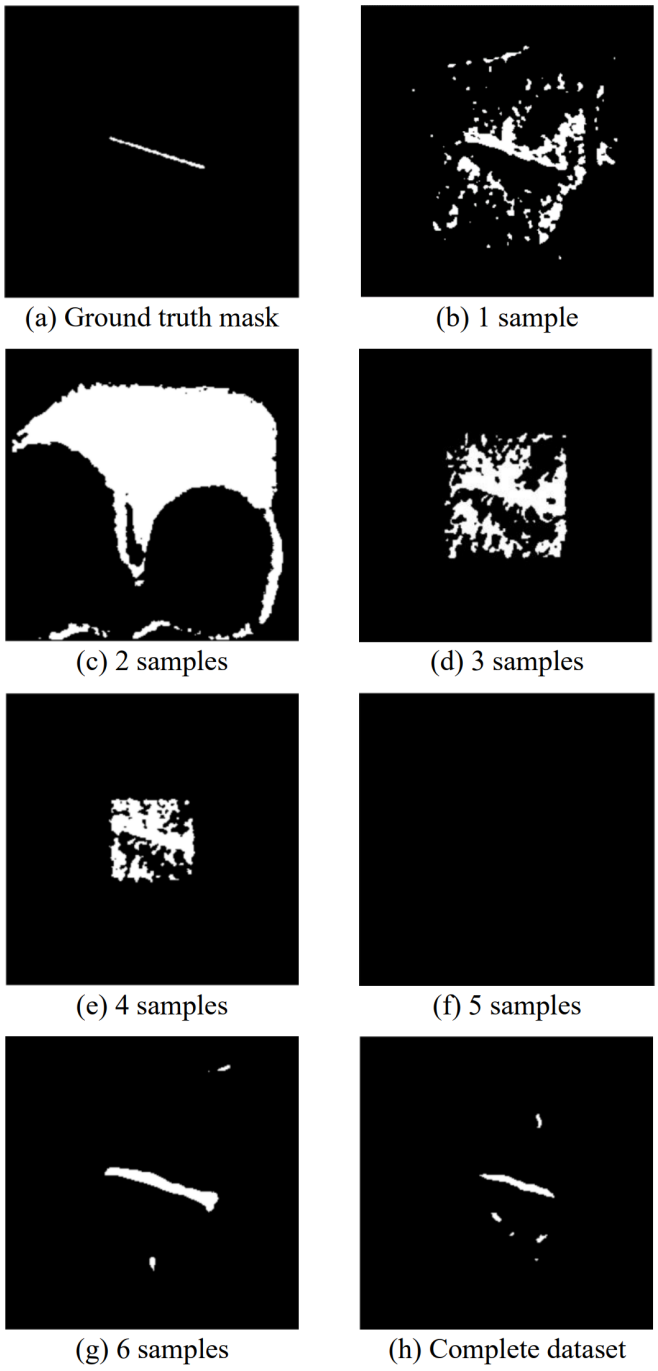

Fig. 6. Ground Truth mask and comparison of network predictions with different numbers of samples per airstrip.

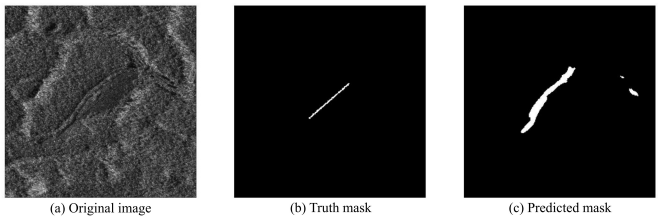

Fig. 7. Example of an unsuccessful detection.

IV. Conclusion

The results presented in this study demonstrate the feasibility of using the U-Net architecture for automatic detection of airstrips in the Amazon region, using X-band SAR imagery from satellites. Despite the limited number of available images, satisfactory results were achieved, indicating that the model can learn distinctive airstrip characteristics even in a data-scarce scenario. The use of lower-resolution images proved to be a viable strategy, allowing for a reduction in computational costs and training time without significantly affecting network performance. Furthermore, the importance

of a well-balanced training dataset became evident, as an excess of samples from the same target adversely impacted model performance. This study offers a practical and replicable approach for monitoring airstrips in the Amazon rainforest using SAR imagery, providing insights for future applications in surveillance and environmental protection.

Future work may explore several directions:

- Assessing the impact of different SAR image preprocessing techniques, including filters for speckle noise reduction, to enhance segmentation accuracy.
- Exploring variations of the U-Net architecture and testing other neural network architectures, such as YOLO and U-Net++, among others.
- Investigating the combination of classical detectors (e.g., edge and line detectors) with neural networks to improve detection robustness.
- Expanding the dataset to include images from various sensors and acquisition conditions to evaluate the generalization capabilities of the model.
- Generating binary segmentation masks directly over SAR images, rather than relying on optical references, to improve spatial alignment and reduce annotation uncertainty.
- Integrating the developed solution into an operational system for continuous monitoring.

A. Acknowledgments

This work was supported by several individuals and institutions. We would like to thank the Brazilian Air Force (FAB) and the Institute for Advanced Studies (IEAv), through the Lessonia Project and C2 Project, for providing the SAR imagery and computational resources used in this study. We also thank the Electronic Warfare Competence Center (CCGE). This work was supported by FINEP (grant number 01.22.0581.00), the National Institute of Science and Technology (INCT-Signals), which is funded by Brazil's National Council for Scientific and Technological Development (CNPq) under grant number 406517/2022-3, the Ministry of Science, Technology, and Innovation (MCTI), and the São Paulo Research Foundation (FAPESP) under grant 20/09838-0 (BI0S—Brazilian Institute of Data Science).

REFERÊNCIAS

[1] Ministério da Defesa (Brasil), "Portaria gm-md nº 1.511, de 26 de março de 2024 — aprova a diretriz ministerial para o emprego das forças armadas na terra indígena yanomami," Diário Oficial da União, Seção 1, p. 7, edição 67, publicado em 08 de abril de 2024, March 2024, ativa o Comando Operacional Conjunto Catrimani II para atuar em apoio a ações governamentais na Terra Indígena Yanomami.

[2] Brazilian Air Force. (2025, April) Comando conjunto catrimani ii divulga balanço anual de atuação. Accessed: June 15, 2025. Annual report on Operation Catrimani II in Yanomami Indigenous Territory—fighters, seizures, destroyed clandestine airstrips. [Online]. Available: https://www.fab.mil.br/noticias/mostra/43976/

[3] E. B. Furtado, T. Franchi, L. B. Rodrigues, and G. D. F. Simões, "Asas que Devastam a Amazônia: Uma Análise do Cenário de Pistas de Pouso e Voos Irregulares que Dão Suporte ao Garimpo Ilegal na TI Yanomami," *Revista (RE)DEFINIÇÕES DAS FRONTEIRAS*, vol. 2, no. 6, pp. 16–51, April 2024.

[4] AP News. (2021, March) Tarnished gold: Aircraft, fuel key to illegal amazon mining. Accessed: June 8, 2025. [Online]. Available: https://apnews.com/article/amazon-mining-indigenous-gold-environment-brazil-c30953daa8482e42288ba509fe2e256a

[5] S. P. Aldy and L. R. dos Santos, "Deforestation in the brazilian amazon: Impacts of land use policies," Resources for the Future (RFF), Working Paper 22-22, 2022, accessed: June 8, 2025.

[6] A. Samanta, S. Ganguly, E. Vermote, R. R. Nemani, and R. B. Myneni, "Why is remote sensing of amazon forest greenness so challenging?" *Earth Interactions*, vol. 16, no. 7, pp. 1–14, 2012.

[7] Brazilian Air Force (FAB). (2022, May) FAB lança primeiros satélites do projeto Lessonia-1. Accessed: June 11, 2025. [Online]. Available: https://www.fab.mil.br/noticias/mostra/39179/

[8] Flores-Anderson, Africa and Herndon, K. and Thapa, Rajesh B. and Cherrington, Emil A., *The SAR Handbook: Comprehensive Methodologies for Forest Monitoring and Biomass Estimation*. NASA Earthdata: NASA / USAID SERVIR and SilvaCarbon, 2019, free e-book; "SAR Handbook was created in 2019 as a guide for forest monitoring and biomass estimation with Synthetic Aperture Radar (SAR)".

[9] L. E. Falqueto, R. L. Paes, and A. Passaro, "Knn e rede neural convolucional para o reconhecimento de plataformas de petróleo em imagens sar do sentinel-1," *Spectrum - The Journal of Operational Applications in Defense Areas*, vol. 24, no. 1, pp. 29–33, September 2023.

[10] Z. Huang, Y. Liu, and L. Zhang, "Sar target recognition based on deep learning: A review," *Remote Sensing*, vol. 13, no. 5, p. 1004, 2021.

[11] Y. Zhu, W. Wang, S. Li, and B. Zou, "Ship detection from sar images using deep learning: A survey," *Remote Sensing*, vol. 11, no. 7, p. 786, 2019.

[12] B. Tavus, R. Can, and S. Kocaman, "A cnn-based flood mapping approach using sentinel-1 sar data," *ISPRS Annals of Photogrammetry, Remote Sensing and Spatial Information Sciences*, pp. 549–556, 2022.

[13] L. Gomes, E. Shiguemori, T. Kuck, and D. Irion Alves, "Evaluation of a yolov8-based method for detecting unauthorized airstrips in the amazon rainforest using sar imagery," in *Conference: XLII Simpósio Brasileiro de Telecomunicações e Processamento de Sinais*, 01 2024.

[14] L. da Silva Gomes, "Automatic Detection and Segmentation of Illegal Airstrips in the Amazon Rainforest Using SAR Imagery," Master's thesis, Instituto Tecnológico de Aeronáutica (ITA), São José dos Campos, 2025.

[15] G. R. Pardini, T. N. Kuck, E. H. Shiguemori, M. R. Maximo, G. Dietzsch, and P. Molina, "Multi-stage algorithm for detecting landing strips in the amazon rainforest," *IEEE Geoscience and Remote Sensing Letters*, 2024.

[16] ICEYE, "ICEYE Data Product Specification 6.0.3," https://sar.iceye.com/latest/foundations/OverviewOfSAR/overviewOfSAR/, February 2025, version 6.0.3. Proprietary document detailing ICEYE imaging modes, data products, tasking options, and service levels.

[17] MapBiomas. (2025) O Projeto MapBiomas. Accessed: June 7, 2025. [Online]. Available: https://brasil.mapbiomas.org/o-projeto/

[18] University of Texas at El Paso, "Why 70–80

[19] O. Ronneberger, P. Fischer, and T. Brox, "U-Net: Convolutional Networks for Biomedical Image Segmentation," in *Medical Image Computing and Computer-Assisted Intervention (MICCAI)*. Springer, 2015, pp. 234–241.

[20] T. Falk, D. Mai, R. Bensch, Özgün Çiçek, A. Abdulkadir, Y. Marrakchi, and F. A. Hamprecht, "U-Net: Deep Learning for Cell Counting, Detection, and Morphometry," *Nature Methods*, vol. 16, no. 1, pp. 67–70, 2019.

[21] EITCA Institute. (2024) How does the u-net architecture leverage skip connections to enhance the precision and detail of semantic segmentation outputs, and why are these connections important for backpropagation? Accessed: 2025-06-17. [Online]. Available: https://eitca.org/artificial-intelligence/eitc-ai-adl-advanced-deep-learning/advanced-computer-vision/advanced-models-for-computer-vision/examination-review-advanced-models-for-computer-vision/how-does-the-u-net-architecture-leverage-skip-connections-to-enhance-the-precision-and-detail-of-semantic-segmentation-outputs-and-why-are-these-connections-important-for-backpropagation/

[22] F. Milletari, N. Navab, and S.-A. Ahmadi, "V-net: Fully convolutional neural networks for volumetric medical image segmentation," in *Proceedings of the Fourth International Conference on 3D Vision (3DV)*. Stanford, CA, USA: IEEE, 2016, pp. 565–571.